Stretching and Tunability of Graphene-Based Passive Terahertz Components

Konstantin G. Batrakov,* Nadezhda I. Volynets, Alesia G. Paddubskaya,
Polina P. Kuzhir, Maria Stella Prete, Olivia Pulci, Evgeni Ivanov, Rumiana Kotsilkova,
Tommi Kaplas, and Yuri Svirko

The dependence of transmission/absorption of terahertz (THz) radiation on strain in graphene is investigated experimentally and with the aid of *ab initio* calculations. By applying strain to chosen graphene layer(s), the effective sheet conductance can be fine-tuned to necessary value to design tunable passive THz components (such as shields, filters, polarizers, etc.) utilizing the high absorption ability of graphene. The positive influence of non-perfectness of chemically vapor deposited (CVD) graphene for strong tunability versus mechanical deformations is also discussed.

1. Introduction

Our daily life heavily relies on sunlight. However, the spectrum of the electromagnetic (EM) waves we use is much broader. It spans from 50/60 Hz, the frequency of the power supply in our households, to X-rays, which we use for routine medical screening. This vast range includes microwave

Dr. K. G. Batrakov, N. I. Volynets, A. G. Paddubskaya, Dr. P. P. Kuzhir
Research Institute for Nuclear Problems
Belarusian State University
Minsk 220006, Belarus
E-mail: kgbatrakov@gmail.com

Dr. K. G. Batrakov, A. G. Paddubskaya, Dr. P. P. Kuzhir
Tomsk State University
Tomsk 634050, Russia

Dr. M. S. Prete, Prof. O. Pulci
Department of Physics, and INFN
University of Rome Tor Vergata
Rome, Italy

Prof. E. Ivanov, Prof. R. Kotsilkova
Institute of Mechanics
Bulgarian Academy of Science
Sofia, Bulgaria

Dr. T. Kaplas
Department of Optoelectronics
Center for Physical Sciences and Technology
Saulėtekio av. 3, LT-10257 Vilnius, Lithuania

Dr. T. Kaplas, Prof. Y. Svirko
Department of Physics and Mathematics
University of Eastern Finland
Joensuu FI-80101, Finland

The ORCID identification number(s) for the author(s) of this article can be found under https://doi.org/10.1002/pssb.201800683.

(communication), infrared (night vision) and optical waves. Nevertheless, there exists a narrow band between microwave and infrared that has been not in use until recently. This is the so-called Terahertz (THz) gap, which is still hardly reachable by either electronic or optical devices. This frequency range corresponds to the temperature of biological processes and covers a substantial fraction of the luminosity from the Big Bang. The emergence of novel THz sources, such as quantum cascade lasers, opened the path to the exploitation of THz waves.[1] The growing interest over the past 10 years in THz science is due to its many important applications in physics, astronomy, chemistry, biology, and medicine, including THz imaging, microscopy, non-destructive testing, tomography, medical diagnosis, health monitoring, environmental control, chemical and biological identification, and in future communication networks. These applications require efficient, durable, robust, and tunable components capable of generating, manipulating, and detecting of THz radiation.[2] According to the just published *The 2017 terahertz science and technology roadmap*[3] among the most important challenges are passive quasi-optical components, i.e., filters, polarizers, collimators, and modulators.

Conventional optical components can be used in the THz range. However, the performances of THz quasi-optics have not reached the same levels as at optical, much shorter, wavelengths. Most popular material solution for passive components at THz is silicon. However, since the undoped Si possesses a high refractive index, 3.41 at THz, Si/air interface reflects 32% of the incident radiation thus decreasing significantly the efficiency of filters, polarizers, etc. What is more, the main drawback of existing THz components is their restricted tunability, which is the must for future THz devices.

Graphene, being light, flexible, and shatterproof, is very attractive to be used in electronic components in post-silicon age. Electromagnetic properties of graphene and its ability to absorb radiation strongly depend on the frequency range, i.e., on which transitions (inter- or intra-band)[4] dominate the graphene *ac* conductivity. In the visual and IR range, graphene monolayer absorbs 2.3% of incident light mainly due to inter-band transitions, while in the THz–subTHz range, the intra-band processes dominate giving rise to absorptance of as high as 20+% per graphene sheet, depending on the doping level.

Recently, we have demonstrated[5] that free standing multilayered structures consisting of alternating graphene monolayers and submicron-thin polymer (PMMA) slabs are capable to absorb up to 50% of the radiation, depending on the number of graphene sheets, thus providing an efficient microwave shielding. According to admittance-matching conditions, in case of using a proper dielectric substrate being 1/4 of wavelength thick,[6] or metamaterials-like type,[7] it is possible to reach almost perfect absorption. The concept of EM components relying on graphene high absorption ability in microwave-THz frequency range has been proposed in our recent work: high performance of graphene in shields, filters, polarizers, operating at the GHz and THz frequencies has also been recently demonstrated.[8]

In order to achieve tunability, we may utilize one of the many outstanding properties of graphene,[9–12] for example its ability to tune the Fermi level with external doping or biasing. Graphene transmission/absorption coefficients depend, in particular, on chemical potential μ.[4,6] For chemical vapor deposition (CVD)-produced graphene, typical values of the chemical potential are $|\mu| \sim 0.1 \div 0.2\,\mathrm{eV}$. Density of carriers and, therefore, graphene sheet conductance depend also on temperature. Hence, transmittance/absorbance can be tuned by temperature variation. However, a rather high variation of temperature is needed for noticeable carrier density altering in CVD graphene.

One more method to tune electronic and optical properties of graphene is to apply mechanical strain or bending.[13,14] In fact, among the many outstanding characteristics, graphene posses also unique mechanical properties with elastic reversible resistance to tensile stress.[15] Landau levels and optical Hall effect have been extensively studied in strained graphene.[16] Effect of strain has been widely investigated with the aim to open a gap (through high shear and uniaxial strain), to produce very strong pseudomagnetic fields (non-uniform strain) and to break the electron-hole symmetry giving rise to a non-isotropic Dirac cone and hence a non-universal IR absorbance for uniaxial strain.[17]

Here, we study the possibility to tune the transmittance ability of graphene/PMMA sandwich structure (i.e., to tune passive THz components relying on the absorbance ability of graphene) with isotropic stretching or strain. Mechanical deformations could be an interesting alternative to other widely applied ways of using external forces to change the chemical potential, mobility and relaxation time of graphene, e.g., electrostatic doping,[18–23] allowing to avoid widely discussed problems of high and non-reproducible metal–graphene contact resistance.[24–31]

2. Theory

As shown in ref. [5], maximal absorptance in graphene corresponds to some optimal value of the effective sheet conductance. Such an optimal value can be reached by combining several graphene layers in sandwich structure.[5,6] Fine-tuning to the exact value of optimal conductance can be fulfilled by applying strain to one of the layers. Sheet conductance depends on the carrier density n, which is connected to the chemical potential μ and relaxation time τ due to carrier scattering processes. The dominant contribution to carrier scattering in supported CVD

graphene (on the substrate, e.g., on the PMMA layer) is due to charge impurities and defects.[32,33] In contrast, in high quality suspended graphene, mobilities exceeding $200\,000\,\mathrm{cm}^2\,\mathrm{V}^{-1}$ are obtained, with main contribution to carrier scattering arising from electron–phonon interaction.

The dependence of chemical potential on strain can be extracted from the considerations below. Carriers density changes with μ following the equation

$$\int \frac{k\,dk}{(2\pi)^2} \frac{g_s g_v}{\exp\{(\varepsilon - \mu)/T\} + 1} = \frac{n_0}{(1 + \sigma)^2} \tag{1}$$

Here g_s, g_v are spin and valley degeneracy, for graphene these parameters equal to two, n_0 is carrier density of unstrained graphene, σ is linear strain, k and ε are electron momentum and energy correspondingly.

In reality, when $|\mu| \gg T$ (typical situation for CVD graphene and room temperature), and $|\mu| \ll t$, where t is graphene hopping parameter, Eq. (1) could be simplified

$$\frac{g_s g_v \mu^2}{2(2\pi)^2 v_F^2} = \frac{n_0}{(1 + \sigma)^2} = \frac{g_s g_v \mu_0^2}{2(2\pi)^2 v_{F0}^2 (1 + \sigma)^2} \tag{2}$$

or

$$\frac{\mu}{\mu_0} = \frac{v_F}{v_{F0}(1 + \sigma)} \tag{3}$$

When deriving (3) the step Dirac–Fermi distribution ($|\mu| \gg T$) and Dirac dispersion law for π electrons in graphene ($|\mu| \ll t$) were used for electrons near the Dirac point. Equation (1) or (3) set the value of the chemical potential, which is necessary for transmission/absorption calculations. v_{F_0} and v_F are Fermi velocities for unstrained and strained graphene, respectively.

Our calculations for the dependence of the Fermi velocity on strain are based on density functional theory (DFT)[34,35] using the Quantum ESPRESSO code.[36] The exchange and correlation functional was selected to be the Perdew–Burke–Ernzerhof (PBE).[37] The calculated Fermi velocities are reported in **Table 1**, together with the lattice constants and work functions. A clear trend is found: by increasing the strain, the Fermi velocities decrease, and the work function increases. Another parameter which influence conductance is relaxation time. Expressions for it, considering that charge impurities give main contribution,

Table 1. Calculated lattice constant (a_{lat}), Fermi velocity, and work function (WF) of graphene for different strain isotropic on the xy plane.

Strain	a_{lat} (A)	v_F ($10^6\,\mathrm{m\,s}^{-1}$)	WF (eV)
0.0	2.460	0.844	4.22
2.2%	2.513	0.819	4.40
2.4%	2.518	0.813	4.42
2.6%	2.523	0.811	4.43
3.5%	2.546	0.805	4.51
4.8%	2.576	0.785	4.61
5.5%	2.595	0.783	4.65

was derived, for example, in ref. [33]

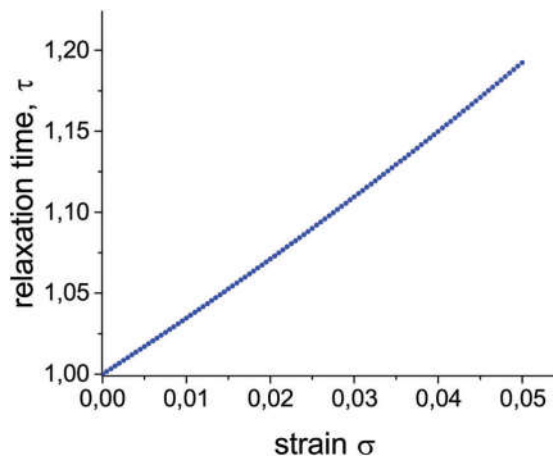$$\frac{1}{\tau} = \frac{n_i}{2\pi\hbar} \left(\frac{2\pi e^2}{\kappa} \right)^2 \frac{2I_0}{\mu} \qquad (4)$$

Here n_i is impurity concentration, k is substrate (or interface) dielectric constant, renormalized by graphene polarization[32]

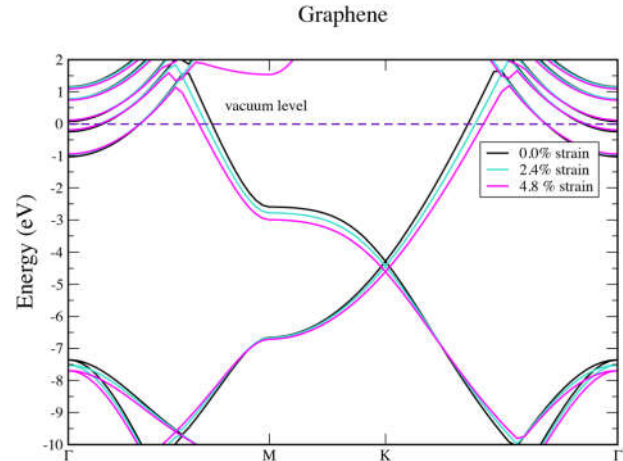$$I_0 = \int_0^1 dx \frac{x^2 \sqrt{1 - x^2}}{(x + 2r_s)^2} \qquad (5)$$

$r_s = e^2/\kappa\hbar v_F$ is graphene fine structure constant. Relaxation time increases with chemical potential (carrier concentration) increase. It is caused by screening effect. Electron cloud screens charged impurities and diminishes long-range scattering. The chemical potential and carrier concentration drop during tensile strain (3). This factor decreases relaxation time. Strain also affects the fine structure constant which increases (because v_F decreases). This factor changes τ in different direction during tensile strain, because decrease of Fermi velocity decreases screening distance. Resulting relaxation time dependence on strain without considering change of impurity concentration can be derived using expressions (3)–(5). **Figure 1** demonstrates dependence of $\tau(\sigma)/\tau_0$ on σ. The dependence for hopping parameter $t = t_0 \exp(-3.37\sigma)$[38] was used. This formula slightly overestimates the effect of strain on hopping parameter.

Table 1 presents *ab initio* calculation for some values of strain applied isotropically to graphene including 2.2, 2.4, 2.6, 3.5, 4.8, and 5.5% in experiments. The strain produces a change in the Fermi velocity and in the work function (WF). In particular, with increasing strain (and hence, increasing C-C distance) the Fermi velocity decreases (see Table 1). According to our DFT calculations, even in presence of strain, the most stable geometry is still planar (no buckling).

The Dirac cone survives also in presence of the imposed strain (see **Figure 2**). As a consequence, the infrared absorbance (interband transitions), which for linear bands in 2D system tends to the universal constant πa[39–41] (a is the Sommerfeld fine structure constant), does not change with the application of


Figure 2. Electronic band structure of graphene (DFT calculation). The bands for unstrained graphene and for strained graphene (2.4 and 4.8%) have been aligned to the same vacuum level. The Fermi energy (and hence the Work Function) change with changing the applied strain.

strain. Interestingly, there are instead large changes in the absorbance and in the 2D-optical conductivity for higher photon energies (see Figure 2 and **Figure 3**).

3. Experimental Section

Graphene was synthetized by conventional CVD method on a copper foil (25 μm, 99.8% pure) by using a custom-made CVD reactor. The reactor chamber was pumped to vacuum for 1 h to cleanse air and moisture from the chamber. Thereafter, the chamber with the foil was heated to 1000 °C in H_2 flow (5 sccm, 0.1 mbar) and the Cu foil was annealed 30 min at this temperature. After the Cu foil annealing, graphene was synthetized on the foil by injecting CH_4 (5 sccm) together with H_2 (5 sccm) into the chamber. The graphitization part lasted 15 min and afterwards,

Figure 1. Dependence of relaxation time on strain.
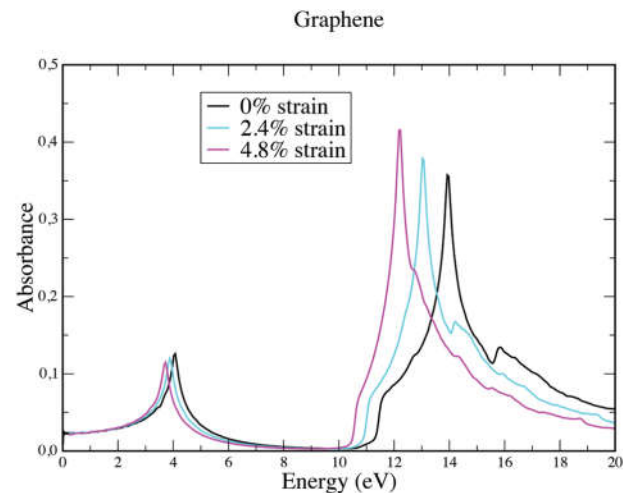
Figure 3. Two-dimensional absorbance for different values of applied strain. Just interband transitions are included.

the chamber was filled with H_2 (10 mbar) and the chamber was cooled down to room temperature (overnight).

The Cu foil with graphene was spin coated with a one micron thick poly(methyl methacrylate) (PMMA) layer, which was cured in 60 C on a hot-plate. The backside of the Cu foil was treated with oxygen plasma (20 s/100 W/20 sccm) to remove graphene layer which was grown on another side of the foil. After removing backside graphene, the Cu foil was etched by $FeCl_3$ solution (overnight). The PMMA-graphene layer was rinsed twice in water before it was attached on a metal plate with a hole (diameter of 10 mm). An adhesion between the PMMA-graphene sandwich and the metal plate was promoted by a double-sided tape around the hole, which allowed us to apply mechanical stress to the sandwich structure.

It is demonstrated from stress-induced Raman bands shifts that stress can be transferred from a polymer matrix to a graphene monolayer in a system polymer/graphene.[42] Here we deal with the same situation.

Terahertz response on isotropic strain was studied. For stretching, contact loading small punch test experiments were done (see for details ref. [43]). Briefly, the Universal Mechanical Testing device UMT-2M (Bruker) with small punch setups (equipped with a very sensitive sensor for load 0.1 mN working in both load control and displacement control modes) was used for macromechanical characterization of the freestanding graphene/PMMA sandwich. The punch diameter was of 6 mm with a spheroidal end shape. **Table 2** presents the load-test details. The graphene/PMMA samples were stretched by 2.2 and 2.6%, respectively.

At THz frequency range, the EM response of unstrained and strained samples has been measured using a commercial THz time-domain spectrometer "T-Spec" by EKSPLA. In a setup photoconductor antenna (low temperature grow GaBiAs), illuminated by ultrashort laser pulses with 1050 nm wavelength, 50–150 fc pulse duration and more than 40 mW output power, was used in order to generate THz radiation up to 2 THz. The THz radiation was focused onto the sample by parabolic mirrors. THz pulses are detected in a similar photoconductive antenna. In order to get better signal to noise ratio (more than 106:1 at 0.4 THz with spectral resolution 5 GHz) up to 1024 scanned curves were averaged for each measurement. This allows us to obtain the experimental error less than 2%. Fourier transformation was used to convert the time-domain signal into the frequency domain.

Table 2. The load-test details.

Sample	Mechanical stretching test details
Graphene/PMMA, 2.2% strain	The Mullins-type 3-step load–upload stretching test runs at 1 mN min^{-1} load rate at 3 steps of increasing load, up to maximum of 6 mN, at 2 min running time for each step. After every load step, a fast upload for 1 s, followed by a hold at 0.3 vmN for 2 min is applied
Graphene/PMMA, 2.6% strain	The 3-step load–hold stretching test runs at 1 mN min^{-1} load rate up to maximum load of 6 mN, as divided in 3 steps of equal load each and 6 min running time. After every load step, a hold at the respective peak load is applied for 2 min

4. Results and Discussion

Figure 4a demonstrates experimental transmission data and calculated ones for unstrained samples and graphene/PMMA stretched by 2.2 and 2.6%. One can see that small strain (stretching) up to 2.6% leads to significant increase of transmittance ability of graphene/PMMA sandwich in THz range (from 62 to 72%).

Comparing experimental data for as-prepared sample with theoretical calculations using expression (3)–(5), one may conclude that concentration of charged impurities in unstrained graphene is about $10^{11}/Z^2\,cm^{-2}$, where Ze is the charge of impurity. The same procedure for strained graphene/PMMA shows that additional micro-defects and impurities appear during the strain as impurities concentration increases by 25% at strain 2.2% and by 40% at 2.6%. It worth noting that within a range of experimental error there is a good agreement between
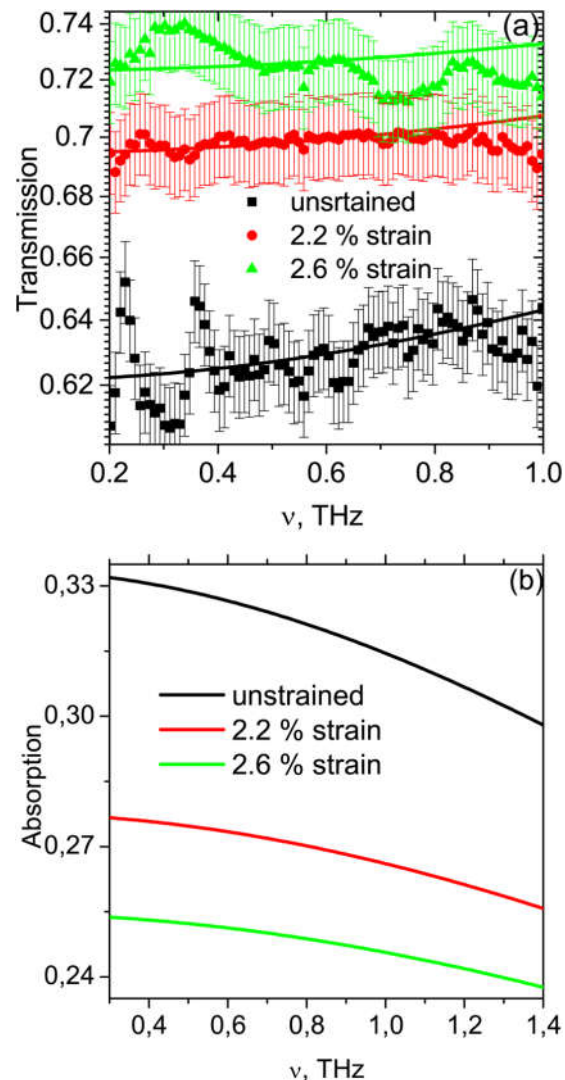
Figure 4. Frequency dependence of the transmittance (a) and absorbance (b); measured (symbols) and calculated values for the graphene of different strain.

transmission spectra measured experimentally and calculated using the theoretical model.

5. Conclusions

Our conclusions are summarized by Figure 4b, which presents calculated absorptance of graphene/PMMA sandwich versus applied strains. The absorbance changes with the applied external forces, from 33% to 23–25%. That is starting from observation of basic principles of mechanically induced tunability concept, we show possibility to tune THz response of passive THz components made of CVD graphene by small mechancal deformations. The importance of CVD graphene imperfectness, i.e., the positive influence of different graphene micro-defects and impurities and their dynamics on the high level of THz graphene tunability at small strain is also addressed, opening the route to cost-effective and efficient processing of tunable passive components necessary for future and emerging THz technologies.

Conflict of Interest

The authors declare no conflict of interest.

[1] B. S. Williams, *Nat. Photon.* **2007**, *1*, 517.
[2] T. Nagatsuma, G. Ducournau, C. C. Renaud, *Nat. Photon.* **2016**, *10*, 371.
[3] S. S. Dhillon, M. S. Vitiello, E. H. Linfield, A. G. Davies, M. C. Hoffmann, J. Booske, C. Paoloni, M. Gensch, P. Weightman, G. P. Williams, E. Castro-Camus, D. R. S. Cumming, F. Simoens, I. Escorcia-Carranza, J. Grant, S. Lucyszyn, M. Kuwata-Gonokami, K. Konishi, M. Koch, C. A. Schmuttenmaer, T. L. Cocker, R. Huber, A. G. Markelz, Z. D. Taylor, V. P. Wallace, J. A. Zeitler, J. Sibik, T. M. Korter, B. Ellison, S. Rea, P. Goldsmith, K. B. Cooper, R. Appleby, D. Pardo, P. G. Huggard, V. Krozer, H. Shams, M. Fice, C. Renaud, A. Seeds, A. Stöhr, M. Naftaly, N. Ridler, R. Clarke, J. E. Cunningham, M. B. Johnston, *J. Phys. D: Appl. Phys.* **2017**, *50*, 043001.
[4] *Carbon Nanotubes and Graphene for Photonic Application* (Eds: J. H. Choi, S. Yamashita, Y. Y. Saito), Woodhead Publishing, Cambridge, UK **2013**.
[5] K. Batrakov, P. Kuzhir, S. Maksimenko, A. Paddubskaya, S. Voronovich, P. Lambin, T. Kaplas, Y. Svirko, *Sci. Rep.* **2014**, *4*, 7191.
[6] K. Batrakov, P. Kuzhir, S. Maksimenko, N. Volynets, S. Voronovich, A. Paddubskaya, G. Valusis, T. Kaplas, Y. Svirko, P. Lambin, *Appl. Phys. Lett.* **2016**, *108*, 123101.
[7] M. Lobet, B. Majerus, L. Henrard, P. Lambin, *Phys. Rev. B* **2016**, *93*, 235424.
[8] P. P. Kuzhir, A. G. Paddubskaya, N. I. Volynets, K. G. Batrakov, T. Kaplas, P. Lamberti, R. Kotsilkova, P. Lambin, *J. Nanophoton.* **2017**, *11*, 032504.
[9] K. S. Novoselov, A. K. Geim, S. V. Morozov, D. Jiang, Y. Zhang, S. V. Dubonos, I. V. Grigorieva, A. A. Firsov, *Science* **2004**, *306*, 666.
[10] S. Das Sarma, S. Adam, E. H. Hwang, E. Rossi, *Rev. Mod. Phys.* **2011**, *83*, 407.
[11] A. J. Frenzel, C. H. Lui, Y. C. Shin, J. Kong, N. Gedik, *Phys. Rev. Lett.* **2014**, *113*, 056602.
[12] L. A. Falkovsky, A. A. Varlamov, *Eur. Phys. J. B* **2007**, *56*, 281.
[13] B. Amorim, A. Cortijo, F. de Juan, A. Grushin, F. Guinea, A. Gutiérrez-Rubio, H. Ochoa, V. Parente, R. Roldan, P. San-Jose, J. Schiefele, M. Sturla, M. Vozmediano, *Phys. Rep.* **2016**, *617*, 1.
[14] V. N. Popov, P. Lambin, *Phys. Rev. B* **2013**, *87*, 155425.
[15] S. Y. Li, K. K. Bai, L. J. Yin, J. B. Qiao, W. X. Wang, L. He, *Phys. Rev. B* **2015**, *92*, 245302.
[16] C. Si, Z. Sun, F. Liu, *Nanoscale* **2016**, *8*, 3207.
[17] V. M. Pereira, R. M. Ribeiro, N. M. R. Peres, A. H. C. Neto, *EPL (Europhys. Lett.)* **2010**, *92*, 67001.
[18] M. Bokdam, P. A. Khomyakov, G. Brocks, Z. Zhong, P. J. Kelly, *Nano Lett.* **2011**, *11*, 4631.
[19] Y. Zhang, V. W. Brar, C. Girit, A. Zettl, M. F. Crommie, *Nat. Phys.* **2009**, *5*, 722.
[20] J. Xue, J. Sanchez-Yamagishi, D. Bulmash, P. Jacquod, A. Deshpande, K. Watanabe, T. Taniguchi, P. Jarillo- Herrero, B. J. LeRoy, *Nat. Mater.* **2011**, *10*, 282.
[21] R. Decker, Y. Wang, V. W. Brar, W. Regan, H. Z. Tsai, Q. Wu, W. Gannett, A. Zettl, M. F. Crommie, *Nano Lett.* **2011**, *11*, 2291.
[22] Y. Zhang, V. W. Brar, F. Wang, C. Girit, Y. Yayon, M. Panlasigui, A. Zettl, M. F. Crommie, *Nat. Phys.* **2008**, *4*, 627.
[23] Y. J. Yu, Y. Zhao, S. Ryu, L. E. Brus, K. S. Kim, P. Kim, *Nano Lett.* **2009**, *9*, 3430.
[24] T. Cusati, G. Fiori, A. Gahoi, V. Passi, M. C. Lemme, A. Fortunelli, G. Iannaccone, *Sci. Rep.* **2017**, *7*, 5109.
[25] H. Liu, H. Kondo, T. Ohno, *Phys. Rev. B* **2012**, *86*, 155434.
[26] S. Kim, J. Nah, I. Jo, D. Shahrjerdi, L. Colombo, Z. Yao, E. Tutuc, S. K. Banerjee, *Appl. Phys. Lett.* **2009**, *94*, 062107.
[27] T. Chu, Z. Chen, *ACS Nano* **2014**, *8*, 3584.
[28] K. Nagashio, T. Nishimura, K. Kita, A. Toriumi, *Appl. Phys. Lett.* **2010**, *97*, 143514.
[29] C. Gong, S. McDonnell, X. Qin, A. Azcatl, H. Dong, Y. J. Chabal, K. Cho, R. M. Wallace, *ACS Nano* **2014**, *8*, 642.
[30] E. J. H. Lee, K. Balasubramanian, R. T. Weitz, M. Burghard, K. Kern, *Nat. Nanotechnol.* **2008**, *3*, 486.
[31] W. S. Leong, H. Gong, J. T. L. Thong, *ACS Nano* **2014**, *8*, 994.
[32] T. Ando, *J. Phys. Soc. Jpn.* **2006**, *75*, 074716.
[33] E. H. Hwang, S. Das Sarma, *Phys. Rev. B* **2009**, *79*, 165404.
[34] P. Hohenberg, W. Kohn, *Phys. Rev.* **1964**, *136*, B864.
[35] W. Kohn, L. J. Sham, *Phys. Rev.* **1965**, *140*, A1133.
[36] P. Giannozzi, S. Baroni, N. Bonini, M. Calandra, R. Car, C. Cavazzoni, D. Ceresoli, G. L. Chiarotti, M. Cococcioni, I. Dabo, A. Dal Corso, S. de Gironcoli, S. Fabris, G. Fratesi, R. Gebauer, U. Gerstmann, C. Gougoussis, A. Kokalj, M. Lazzeri, L. Martin-Samos, N. Marzari, F. Mauri, R. Mazzarello, S. Paolini, A. Pasquarello, L. Paulatto, C. Sbraccia, S. Scandolo, G. Sclauzero, A. P. Seitsonen, A. Smogunov, P. Umari, R. M. Wentzcovitch, *J. Phys.: Condens. Matter* **2009**, *21*, 395502.
[37] J. P. Perdew, K. Burke, M. Ernzerhof, *Phys. Rev. Lett.* **1996**, *77*, 3865.

[38] V. M. Pereira, A. H. Castro Neto, N. M. R. Peres, *Phys. Rev. B* **2009**, *80*, 045401.

[39] R. R. Nair, P. Blake, A. N. Grigorenko, K. S. Novoselov, T. J. Booth, T. Stauber, N. M. R. Peres, A. K. Geim, *Science* **2008**, *320*, 1308.

[40] F. Bechstedt, L. Matthes, P. Gori, O. Pulci, *Appl. Phys. Lett.* **2012**, *100*, 261906.

[41] L. Matthes, P. Gori, O. Pulci, F. Bechstedt, *Phys. Rev. B* **2013**, *87*, 035438.

[42] L. Gong, I. A. Kinloch, R. J. Young, I. Riaz, R. Jalil, K. S. Novoselov, *Adv. Mater.* **2010**, *22*, 2694.

[43] R. Kotsilkova, P. Todorov, E. Ivanov, T. Kaplas, Y. Svirko, A. Paddubskaya, P. Kuzhir, *Carbon* **2016**, *100*, 355.